Available online at www.sciencedirect.com
ScienceDirect
Trans. Nonferrous Met. Soc. China 27(2017) 1608−1617
Transactions of Nonferrous Metals Society of China
www.tnmsc.cn

Dynamic mechanical properties and instability behavior of layered backfill under intermediate strain rates

Yun-hai ZHANG, Xin-min WANG, Chong WEI, Qin-li ZHANG

School of Resources and Safety Engineering, Central South University, Changsha 410083, China

Received 11 April 2016; accepted 19 October 2016

Abstract: To obtain dynamic mechanical properties and failure rule of layered backfill under strain rates from 10 to 80 s^{-1}, impact loading test on layered backfill specimens (LBS) was conducted by using split Hopkinson pressure bar system. The results indicate that positive correlation can be found between dynamic compressive strength and strain rate, as well as between strength increase factor and strain rate. Dynamic compressive strength of LBS gets higher as the arithmetic average cement−sand ratio increases. Compared with static compressive strength, dynamic compressive strength of LBS is enhanced by 11% to 163%. In addition, the energy dissipating rate of LBS lies between that of corresponding single specimens, and it decreases as the average cement content increases. Deformation of LBS shows obvious discontinuity, deformation degree of lower strength part of LBS is generally higher than that of higher strength part. A revised brittle fracture criterion based on the Stenerding−Lehnigk criterion is applied to analyzing the fracture status of LBS, and the average relevant errors of the 3 groups between the test results and calculation results are 4.80%, 3.89% and 4.66%, respectively.

Key words: layered backfill specimen (LBS); split Hopkinson pressure bar (SHPB); dynamic mechanical properties; damage characteristic; failure criterion

1 Introduction

Due to the relatively low-level dilution ratio and flexibility, cut and fill stoping method is widely adopted in underground mines. To reinforce the working-face, reinforced backfill layer with higher strength is paved above the general backfill, thus backfill body presents a layered structure [1]. In Sijiaying Iron Mine (SIM), for example, under the condition of the same mass concentration of 72% and curing time of 28 d, the adopted cement−sand mass ratio of general backfill layer is 1:12 while that is 1:4 for the reinforced backfill layer, the maximum compressive strength of latter concreted backfill is 2.2 MPa, which is almost two and a half times that of the former. When excavation equipment works on the surface of concreted backfill body, or blasting operation of adjacent stope is under execution, dynamic load will be exerted on the layered backfill body. Due to different characteristics of backfill layers such as mass fraction, cement−sand mass ratio and porosity, the failure sensitivities of backfill layers to certain strain rate are distinctly diverse, dynamic load working on these backfill layers may lead to different levels of failure. It is unreliable to estimate the stability of layered backfill body on stopping site by using static mechanical properties obtained from common compression test on single structure specimens. Thus, dynamic failure strength should be regarded as an important reference to estimate the stability of layered backfill body under dynamic disturbance and complex deep mine environment [2]. However, no norm about dynamic mechanical properties of layered backfill has been taken into account in any mines. And there are few correlational studies on such issue. So far, several studies on the dynamic mechanism of layered concrete material have been implemented. DONG et al [3] analyzed the influence of dynamic stress on multi-layered media and pointed out that inferior constituent part of multi-layered media is the key factor which leads to deformation. LIU et al [4] studied the damage constitutive relation of stratified composite concrete and derived the damage evolution equation under different conditions. And several stability criterions of backfill body by associating

Foundation item: Project (2012BAC09B02) supported by the 12th Five-Year Key Programs for Science and Technology Development of China; Project (2016zzts444) supported by the Financial Support from the Fundament Research Funds for the Central Universities of Central South University, China

Corresponding author: Xin-min WANG; Tel: +86-731-88879821; E-mail: wxm1958@126.com

DOI: 10.1016/S1003-6326(17)60183-3

dynamic stress rate method with the rule of blasting vibration attenuation have been summarized [5−7].

Split Hopkinson pressure bar (SHPB) system has been extensively used in dynamic properties research of rock and concrete material [8−10]. By using the SHBP system, KUMAR [11] and RINEHART [12] found out that dynamic strength of rock increased with the increase of strain rate. XIAO and ZHANG [13] noticed that the growth rate of compressive strength and the critical strain both had linear relationship with strain rate when strain rates ranged from 1.0×10^{-5} to 1.0×10^{-2} s^{-1}. BISCHOFF and PERRY [14] carried out the uniaxial compression test on concrete under strain rates of 5 to 10 s^{-1}, and the results proved that dynamic strength of concrete was 50% to 60% higher compared with static strength. OLSSON [15] found out that the growth rate of dynamic compressive strength of tuff was enlarged significantly under certain strain rate. In addition, SHPB system can also provide dynamic load on backfill specimens with strain rates of 10 to 90 s^{-1} to simulate the vibration caused by working equipment and blasting [16,17]. Furthermore, TEDESCO and ROSS [18] summarized the empirical formula of determining dynamic strength augment by synthesizing both the static and dynamic compression tests on concrete, and the formula indicates that dynamic strength of concrete increased rapidly when strain rate was over 63.1 s^{-1}.

Nevertheless, all the researches mentioned above are mostly about the dynamic mechanical properties of concrete and rock, research on dynamic mechanical properties of layered backfill is completely scarce. Consequently, to eliminate the gap and provide a theory basis of stability analysis of layered backfill under dynamic disturbance, researches on such area are extremely urgent. In this work, layered backfill specimen (LBS) was made and impact test on these specimens by using SHPB system was conducted. Furthermore, a cylindrical finite element model was constructed to simulate the stress and displacement status of LBS by the application of Flac3D. Analysis of micro-mechanism of LBS by scanning electron microscopy (SEM) was used to interpret the macro-dynamic mechanism of layered backfill.

2 Experimental

2.1 Material

The tailing materials were derived from SIM, Hebei, China, an iron mine with ultra-large production capacity. To obtain representative material samples for test, ingredient tailings were homogeneously mixed on the basis of the corresponding yields.

Particle size distribution was determined by Mastersizer−3000 laser particle analyzer, and the results are tabulated in Table 1. Cumulative mass fraction of particles whose sizes are small than 75 μm is 83.0% and the median size is 0.019 mm, relatively small, large amounts of fine particles will distinctly impair the strength of backfill body. Based on the compression test, compression coefficient and compression modulus of tested tailings were identified under varying loadings, the results are listed in Table 2. When load ranges from 100 to 200 kPa, the compression coefficient is about 0.83 and corresponding compression modulus is 2.90 MPa, the tailings present comparatively high compressibility.

Table 1 Particle size distribution of tailings

Size/μm	Distribution/%
500	7.6
250−500	6.8
75−250	2.6
50−75	6.1
5−50	63.2
<5	13.7
D_{50}	19

D_{50} is median size.

Table 2 Compressibility coefficient and compression modulus of tailings

Loading/kPa	Compressibility coefficient	Compression modulus/MPa
0−50	5.40	0.44
50−100	1.10	2.22
100−200	0.83	2.90
200−400	0.38	6.34

2.2 Fabrication of layered backfill specimen

LBS is a combination of at least two layers of backfill specimens with different characteristics. In this work, as shown in Fig. 1, two-layered LBS was adopted.

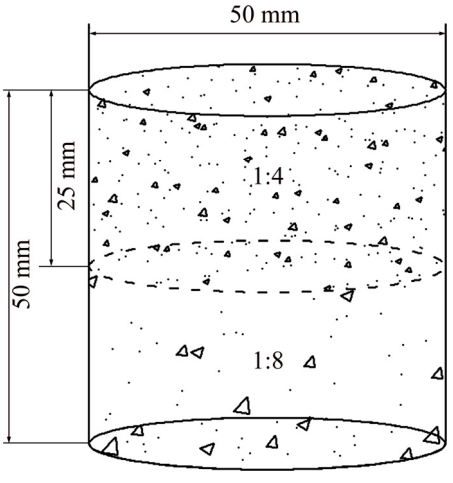

Fig. 1 Schematic diagram of LBS

The making process of layered backfill specimens is as follows: Step 1, put tailings, binder (ordinary Portland cement, #32.5) and water with certain dosage into electrical blender and mix them homogenously; Step 2, rapidly pour the well-mixed slurry with specific cement−sand ratio into mold (*d*50 mm × 50 mm) of half volume in advance, after two or more hours, fulfill the mold with slurry of another adopted cement−sand mass ratio; Step 3, when specimens are initially set (general initial setting time of slurry is about 20 h), demold specimens with an air-pressure extruder and place specimens into curing box at temperature of 18 °C with humidity of 95%.

The adopted cement−sand mass ratios of single backfill specimens are 1:4, 1:6 and 1:8, and the combined cement−sand ratios of LBS are 1:4−1:8, 1:4−1:12 and 1:8−1:12, respectively, while the mass concentration of all the specimens is 72%. In this experiment, 180 specimens including single backfill specimens and LBS were made. The details of prepared specimens are summarized in Table 3.

2.3 Dynamic compression test

Dynamic compression test was conducted on specimens when the curing time was up to 28 d. Because the strain rate provided by split Hopkinson pressure bar (SHPB) system is identical to that of excavation equipment and blasting [19], the 50 mm-diameter SHPB was adopted as the impact loading equipment and provided dynamic impact with intermediate strain rates (10 to 80 s^{-1}) by controlling the pressure of power gas (Table 3). Figure 2 shows the equivalent structure diagram of SHPB system.

3 Results and discussion

3.1 Dynamic compressive strength of LBS

When the curing period of backfill specimens was up to 28 d, dynamic mechanism of test specimens was determined by SHPB under strain rates from 10 to 80 s^{-1}. Dynamic properties and energy parameters were obtained based on the wave signals, and several representative results are listed in Table 4.

Table 3 Scheme of mix parameters of prepared specimens and test conditions

Sample	Cement−sand ratio	Binder content/%	Mass concentration/%	Curing time/d	Loading pressure/MPa
A_i	1:4	14.4	72	28	0.32,0.35,0.40,0.45
Bi	1:8	8.0	72	28	0.35,0.38,0.40,0.42
C_i	1:12	5.53	72	28	0.30,0.33,0.36,0.38
AB_i	1:4−1:8	11.2	72	28	0.32,0.35,0.36,0.38,0.40,0.45
AC_i	1:4−1:12	9.97	72	28	0.30,0.32,0.35,0.38,0.42
BC_i	1:8−1:12	6.76	72	28	0.30,0.32,0.35,0.38,0.40

Table 4 Representative results of dynamic properties of backfill specimens

Sample	Cement−sand ratio	Strain rate/s^{-1}	Peak strength/MPa	Peak strain	Elasticity modulus/GPa	DSIF
AB_{1-1}	1:4−1:8	15	1.020	0.0021	9.8	1.11
AB_{4-2}	1:4−1:8	64	5.319	0.0051	44.1	2.46
AB_{6-1}	1:4−1:8	74	6.008	0.0053	50.7	2.61
AC_{2-2}	1:4−1:12	19	0.825	0.0020	9.9	1.21
AC_{4-2}	1:4−1:12	64	4.052	0.0049	45.7	2.51
AC_{6-1}	1:4−1:12	74	5.213	0.0055	50.9	2.59
BC_{1-1}	1:8−1:12	15	0.381	0.0006	7.2	1.18
BC_{6-2}	1:8−1:12	75	4.479	0.1290	49.7	2.63

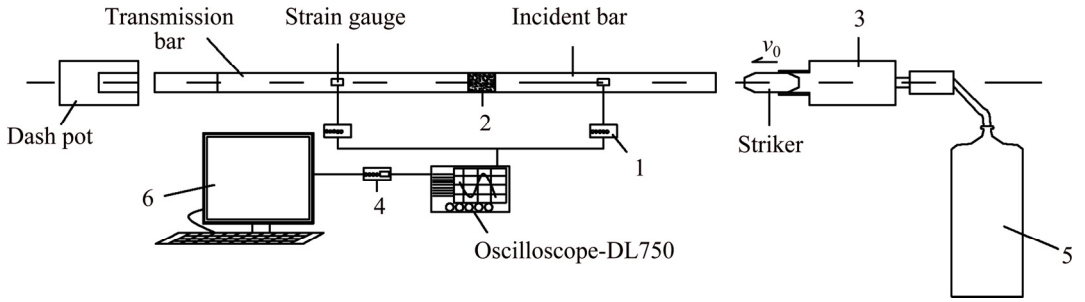

Fig. 2 Schematic diagram of split Hopkinson pressure bar system: 1—Signal amplifier; 2—Tested specimen; 3—Pressure vessel; 4—Signal converter; 5—Gas tank; 6—Computer

In Table 4, it can be seen that group AB of LBS, whose combined cement−sand ratios are 1:4−1:8, gains growth maximal of dynamic compressive strength from 1.020 to 6.008 MPa, and the corresponding elasticity modulus increases from 9.8 to 50.74 GPa. Group BC of LBS, whose combined cement−sand ratios are 1:8−1:12, obtains minimum growth of dynamic compressive strength from 0.381 to 4.479 MPa, and the corresponding elasticity modulus increases from 7.2 to 49.72 GPa. Meanwhile, it can be seen from Fig. 3 that dynamic compressive strengths of the three LBS groups at the same strain rate are in the order: group AB (1:4−1:8) > group AC (1:4−1:12) > group BC (1:8−1:12). It can be concluded that dynamic compressive strength of LBS will be larger when average cement content gets higher.

As seen in Fig. 3, dynamic compressive strengths of the three LBS groups have evident larger growth rates in comparison to that of corresponding single backfill specimens. It can also be noted that the curves of each group of LBS and the corresponding single backfill specimens have two intersections. When strain rate is below 48 s^{-1} (denoted as former intersected strain rate), dynamic compressive strength of group AB of LBS is slightly lower than that of single backfill specimen A, whose strength is lower between the two corresponding single backfill specimens. When the strain rate is over

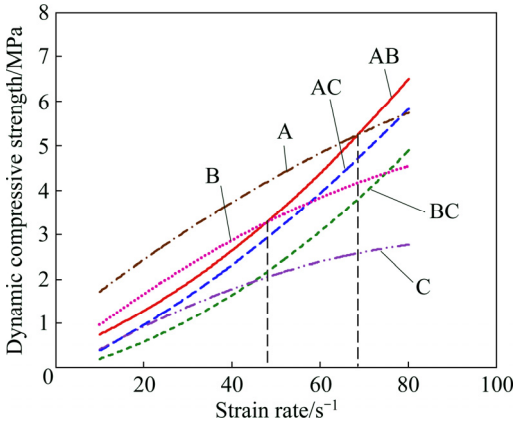

Fig. 3 Fitting curves of dynamic compressive strength of backfill specimens

69 s^{-1} (denoted as latter intersected strain rate), dynamic compressive strength of group AB of LBS becomes clearly higher than that of single backfill specimen B, whose strength is higher between the two corresponding single backfill specimens. The similar phenomena can also be obtained from groups AC and BC of LBS, and strain rates attach to former and latter intersection of groups AC and BC of LBS are 16 s^{-1}, 79 s^{-1} and 45 s^{-1}, 75 s^{-1}, respectively.

From Fig. 4, a positive correlation between dynamic strength increase factor (DSIF) and strain rate can be

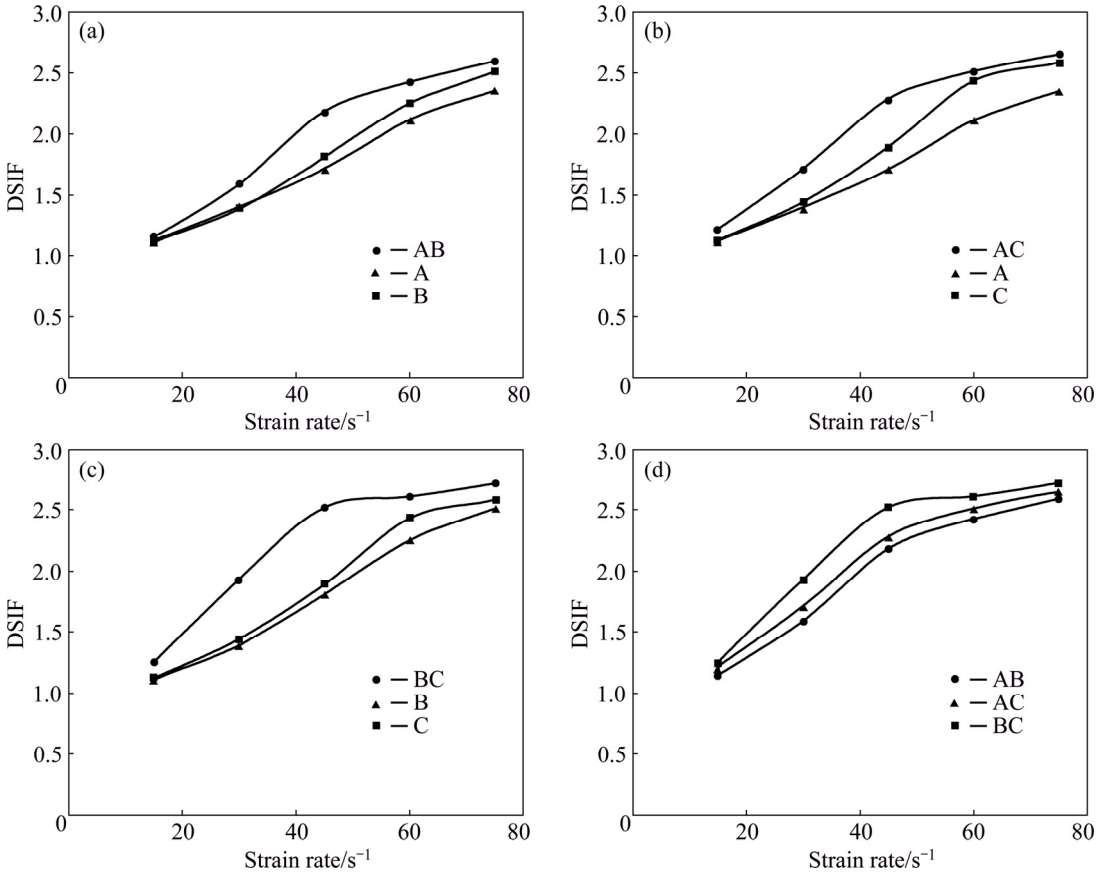

Fig. 4 Curves of DSIF of backfill specimens

found, and DSIF of all specimens range within 1.11−2.63. In other words, compared with static compressive strength, dynamic compressive strength of LBS is enhanced by 11% to 163% when strain rate increased from 10 to 80 s^{-1}. Figures 4(a)−(c) show that DSIF of LBS is a little higher than that of corresponding single backfill specimens. Figure 4(d) presents that DSIF of LBS with specific combined cement−sand ratio is in the order of group BC (1:8−1:12) > group AC (1:4−1:12) > group AB (1:4−1:8), which indicates that the DSIF increases as the average cement content of LBS decreases.

3.2 Energy variation of LBS

The effects of impacts on backfill specimens are presented as energy variation through stress wave propagating. At the contact face of specimen and iron bar, incident energy (E_I) breaks up into reflected energy (E_R) and transmitted energy (E_T). And energy transmitted into specimen will be partly dissipated and causes damage to specimen. Energy of each phase can be obtained from following equations [20], and results are listed in Table 5. SEA in Table 5 is abbreviation of specific energy absorption.

$$E_I = \frac{A_e c_e}{E_e}\int_0^t \sigma_I^2(t)\mathrm{d}t \quad (1)$$

$$E_R = \frac{A_e c_e}{E_e}\int_0^t \sigma_R^2(t)\mathrm{d}t \quad (2)$$

$$E_T = \frac{A_e c_e}{E_e}\int_0^t \sigma_T^2(t)\mathrm{d}t \quad (3)$$

$$E_A = E_I - E_R - E_T \quad (4)$$

where A_e is the cross sectional area of backfill specimen, c_e is the velocity of stress wave in iron bar, E_e is the elasticity modulus of specimen, moreover, σ_I, σ_R and σ_T represent the incident stress, reflected stress and transmitted stress, respectively.

From Fig. 5, it can be seen that incident energy and energy dissipation rate of each specimen both increase as strain rate increases from 10 to 80 s^{-1}. As seen in Figs. 5(a)−(c), incident energy of LBS lies between that of the corresponding single backfill specimens while the energy dissipation rate of LBS is higher than that of corresponding single backfill specimens. Due to the different strengths of the two parts of LBS, stress wave reflects several times at the interface of the two parts and causes increment of energy dissipation. Figure 5(d) shows that incident energy and energy dissipation rate of LBS under the same strain rate are both in the order of group BC (1:8−1:12) > group AC (1:4−1:12) > group AB (1:4−1:8), which indicates that incident energy and energy dissipation rate will get higher when average cement content of LBS is less.

3.3 Microstructural characterization of specimens

The microstructures of specimens with different cement−sand ratios are nearly same. Figure 6 shows the

Table 5 Energy variation of backfill specimen

Sample	Cement−sand ratio	Strain rate/s^{-1}	Incident energy/J	Reflected energy/J	Transmission energy/J	Absorbed energy/J	SEA/($J\cdot cm^{-3}$)	Energy dissipation rate/%
AB_1	1:4−1:8	15	8.12	8.01	0.003	0.107	0.00109	1.317
AB_2	1:4−1:8	20	12.23	12.02	0.004	0.206	0.00209	1.684
AB_3	1:4−1:8	30	20.01	19.53	0.005	0.475	0.00484	2.374
AB_4	1:4−1:8	45	33.63	32.49	0.011	1.132	0.01153	3.431
AB_5	1:4−1:8	60	35.78	34.45	0.050	1.280	0.01303	3.577
AB_6	1:4−1:8	74	37.61	36.18	0.060	1.370	0.01477	3.855
AC_1	1:4−1:12	15	9.75	9.60	0.009	0.140	0.00142	1.435
AC_2	1:4−1:12	30	22.50	21.92	0.011	0.568	0.00578	2.524
AC_3	1:4−1:12	45	33.11	31.89	0.011	1.213	0.01235	3.663
AC_4	1:4−1:12	53	36.78	35.35	0.015	1.415	0.01441	3.847
AC_5	1:4−1:12	60	38.52	36.95	0.018	1.548	0.01576	4.018
AC_6	1:4−1:12	74	41.95	40.16	0.021	1.763	0.01795	4.202
BC_1	1:8−1:12	15	9.97	9.82	0.001	0.149	0.00151	1.490
BC_2	1:8−1:12	30	23.33	22.71	0.001	0.618	0.00629	2.650
BC_3	1:8−1:12	45	36.91	35.50	0.002	1.407	0.01433	3.813
BC_4	1:8−1:12	52	40.02	38.47	0.004	1.546	0.01575	3.863
BC_5	1:8−1:12	60	42.02	40.27	0.003	1.746	0.01779	4.157
BC_6	1:8−1:12	79	47.19	45.10	0.048	2.042	0.02079	4.327

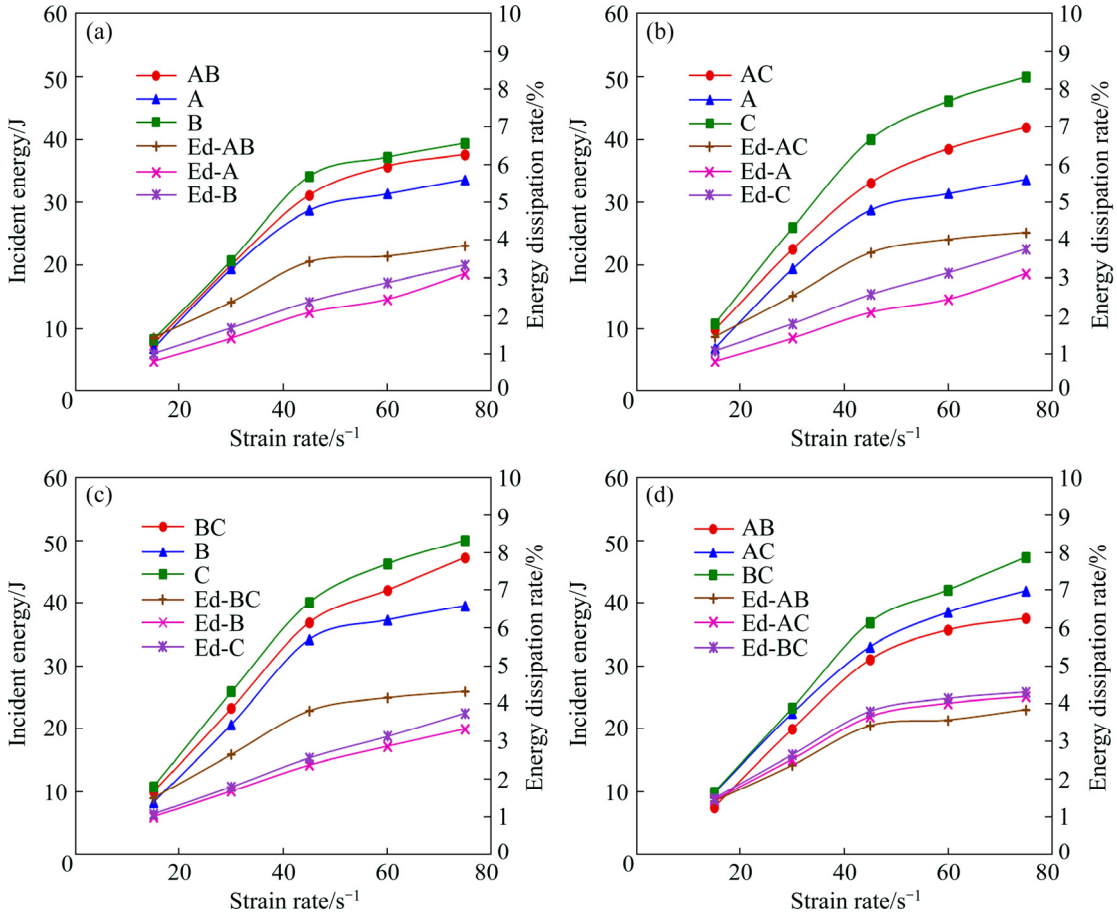

Fig. 5 Curves of incident energy and energy dissipation (Ed) rate of backfill specimens

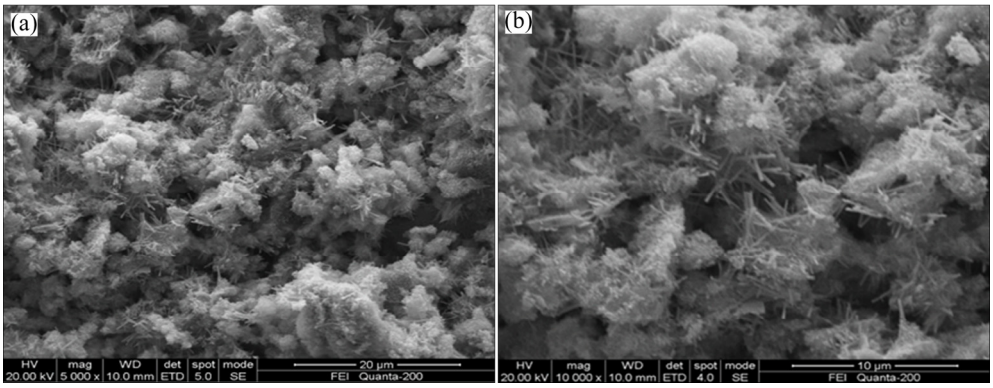

Fig. 6 SEM images of test backfill

SEM images of backfill with magnification of 5000 times and 10000 times, respectively. Figure 7 shows the EDS spectrum of contained elements.

After curing period of 28 d, large amounts of calcium−aluminate compounds have been generated through hydration reaction of silicates. Ettringite ($3CaO{\cdot}Al_2O_3{\cdot}3CaSO_4{\cdot}32H_2O$), the major hydration product, has a decisive influence on the strength of LBS. As shown in the SEM and EDS images, the acicular crystal ettringite aggregated through solid phase reaction when the Ca^{2+} is oversaturated (pH value is over 13.9). A mass of voids have been formed among the intercrossed acicular crystal structure, which stores more inflation pressure and leads to high compressibility of test specimens of about 120%; however, acicular crystal ettringite enlarges the contact area of tailing particles, and then enhances the compressive strength of test specimens. Though some experimental literatures indicate that ettringite begins to decompose when temperature is over 75 °C, and then disorganized backfill [21], the current temperature in underground mines is below 75 °C, temperature effects on strength of

backfills comprised of such tailings can be ignored.

Figure 8 shows that the microstructures of interface region of LBS, discontinuous gap and several unsealed pores are exposed to the electron microscope. Such pore configuration at the interface causes reflection of dynamic stress wave, enlarges the wave resistance and impairs strength of LBS, all these adverse factors have conspicuous effects on the stability of layered backfill body. This makes sense that the strength of layered backfill block is generally weaker than that of single backfill block. In mining situ, pore configuration is a common phenomenon under current circumstance of backfill technology. Thus, improving the backfill technology to completely eradicate or partly reduce pores in backfill body is imperatively demanded.

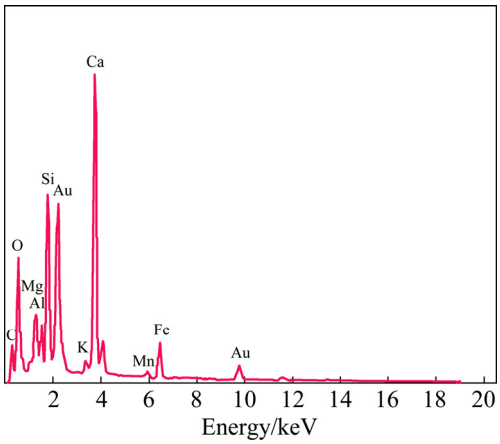

Fig. 7 EDS results of sample tailings

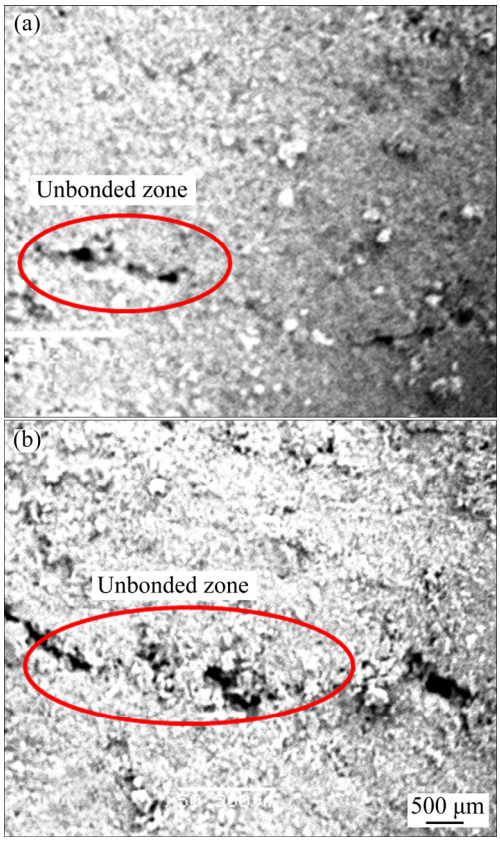

Fig. 8 SEM images of LBS surface in bond region: (a) Well-bonded interface; (b) Poorly-bonded interface

3.4 Damage pattern of LBS

Along with dissipation of stress wave and energy, micro-cracks inside LBS develop rapidly and cause macroscopic damage to specimens eventually. Analysis results of damage degree and damage mode of LBS can be used for qualitative evaluation about energy consumption mechanism and unloading condition of backfill body, and this contributes to enhance the safety management of working site.

From Fig. 9, it can be seen that cracks mainly developed along the axial direction of LBS, which can be attributed to the Poisson effect, and tensile stress along the lateral direction of specimen under impact was brought out. It can also be noted that cracks merely appear on the side face of group AB of LBS when the strain rate is 20 s^{-1}, and specimen AB_6 was completely smashed when the strain rate is 74 s^{-1}. As for group AC of LBS, cracks accompanied by partial spalling appear when strain rate is 45 s^{-1}, and specimen AC_6 is broken up into several fragment when strain rate is 74 s^{-1}. And the lumpiness of specimen AC_6 is bigger than that of specimen AB_6. This indicates that stability of group AB of LBS with higher average cement−sand ratio is more sensitive to strain rate than group AC of LBS. Through analysis on the structure of LBS, critical failure strain rates of single backfill specimens A and B are comparatively similar. When AB of LBS begins to be failure under dynamic impact, single backfill specimens A and B are both to be failure, which facilitates the development of axial cracks across the whole LBS. However, critical failure strain rate of single backfill specimen C is obviously lower than that of specimen A. Thus, cracks only appear on component specimen C while component specimen A is nearly intact as shown in Fig. 9(d).

Figure 10 shows the numerical simulation of radial displacement distribution of LBS at strain rate of 50 s^{-1} by Flac3D. In the deformation distribution nephogram, radial displacement of LBS primarily emerges at bottom part whose strength is comparatively lower than that of top part. The dark color region indicates larger deformation appears, in Fig. 10(a), deformation of bottom part (cement−sand ratio is 1:8) is more obvious than that of top part (cement−sand ratio is 1:4). In Fig. 10(b), bottom part with cement−sand ratio of 1:12 collapsed while top part with cement-sand ratio of 1:8 remained intact. The conformance degree between numerical simulation results and laboratory experiment

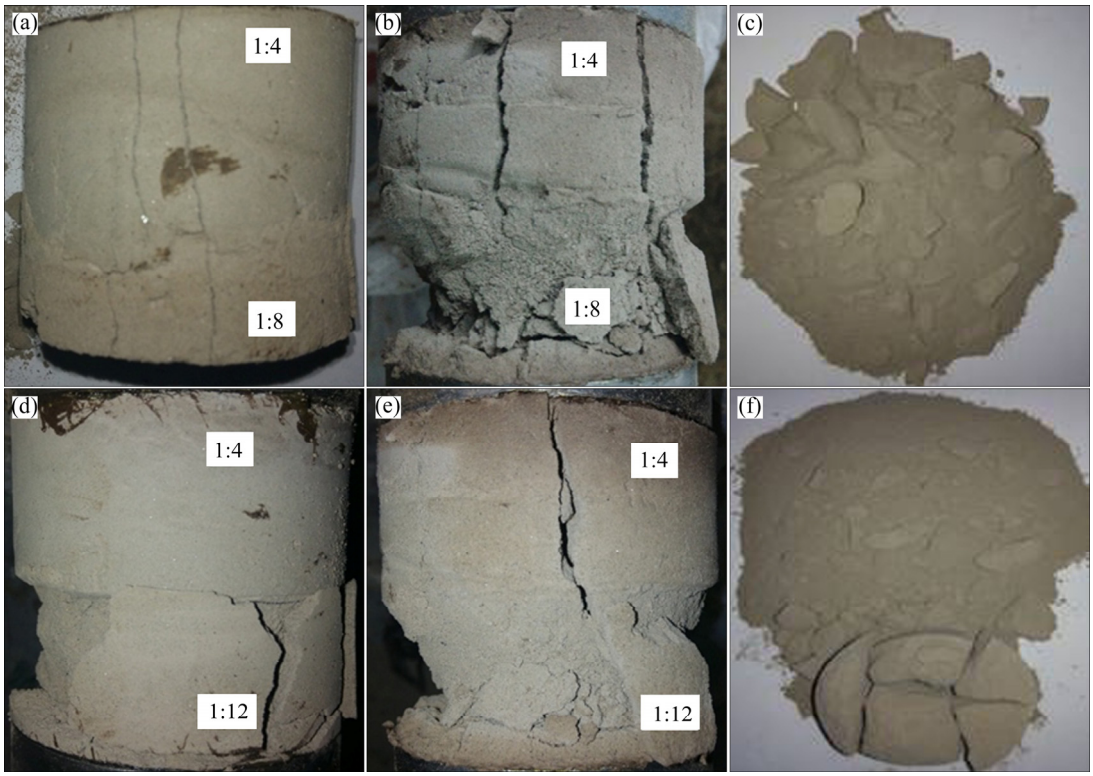

Fig. 9 Damage and smash status of group AB and group AC of LBS: (a) AB_2, $\dot{\varepsilon}$ =20 s^{-1}; (b) AB_5, $\dot{\varepsilon}$ =60 s^{-1}; (c) AB_6, $\dot{\varepsilon}$ =74 s^{-1}; (d) AC_3, $\dot{\varepsilon}$ =45 s^{-1}; (e) AC_5, $\dot{\varepsilon}$ =60 s^{-1}; (f) AC_6, $\dot{\varepsilon}$ =74 s^{-1}

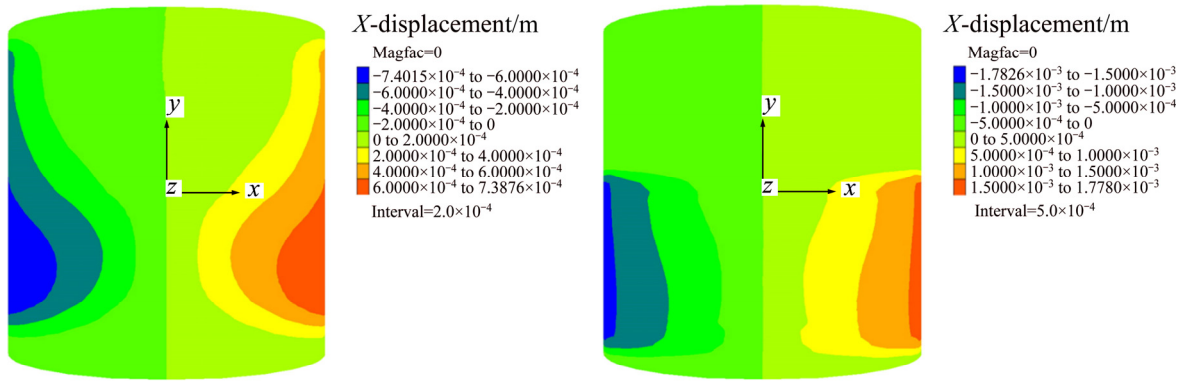

(a) (b)

Fig. 10 Numerical simulation of radial displacement distribution of LBS at strain rate of 50 s^{-1}: (a) Group AB; (b) Group AC

results of radial displacement distribution of LBS is desirable.

3.5 Failure criterion based on energy dissipating

Most experimental study and shock failure theory have summarized that rock failure is generally caused by the tensile stress at the tips of crack [22,23]. Especially, in polycrystalline material, differences of acoustic impedance at the boundary of heterogeneity particles induce partial reflection of stress wave. Hence, compression wave can also cause extension fracture of cracks [24].

When static fracture occurs, for brittle material, Griffith's strength theory has summarized the fracture criterion as [25]

$$\sigma^2 = \frac{2\gamma E}{\pi a} \tag{5}$$

where γ is the specific surface energy of specimen, E is the elasticity modulus of specimen and a is the length of crack.

Based on Griffith's strength theory, STENERDING and LEHNIGK [26] synthesized the amplitude and duration of stress wave, and proposed a formulation to

estimate the occurrence of fracture as follows:

$$\frac{1}{2E}\int_0^{\tau}\sigma^2(t)\mathrm{d}t \geq \frac{k\gamma}{3C} \tag{6}$$

where C is the velocity of stress wave penetrates through specimen, τ is the last time of stress wave, τ=1.1a/C.

For arbitrary stress wave, the dynamic fracture criterion based on the Stenerding−Lehnigk criterion [26] can be rewritten as

$$\int_0^{\tau}\sigma^2(t)\mathrm{d}t \geq \frac{\pi\gamma E}{C} \tag{7}$$

If the energy density of specimen is greater than the value of $\pi\gamma E/C$, cracks will extend with higher velocity, and macroscopic failure of specimen will appear finally.

In view of the difference of wave impedance between the two corresponding single specimens of LBS, wave reflection at the interface of the two parts will affect the duration of stress wave. Thus, a parameter of combined cement−sand ratio is introduced to counteract the effect of different wave impedance, and Eq. (7) can be revised as

$$\int_0^{\tau}\sigma^2(t)\mathrm{d}t \geq \frac{\pi\gamma E}{C}\cdot f(\dot{\varepsilon},\ r_i,\ r_j) \tag{8}$$

$$f(\dot{\varepsilon},\ r_i,\ r_j) = 5.334\exp[\frac{r_j}{(r_i+r_j)}\cdot\dot{\varepsilon}^{-1.241}] \tag{9}$$

where r_i and r_j are the cement−sand ratios of specimens, and j>i.

In order to verify the validation and capability of Eq. (8), contrast between test results and calculation results was carried out, the comparison result is shown in Fig. 11. It can be seen that the fitting curves of calculation results are relatively coincided with test results. The average relative errors of three groups LBS were 4.80%, 3.89% and 4.66% respectively, which are acceptable within permissible error range. In a word, the revised failure criterion based on incident energy is applicative to judge the damage state of LBS in this experiment.

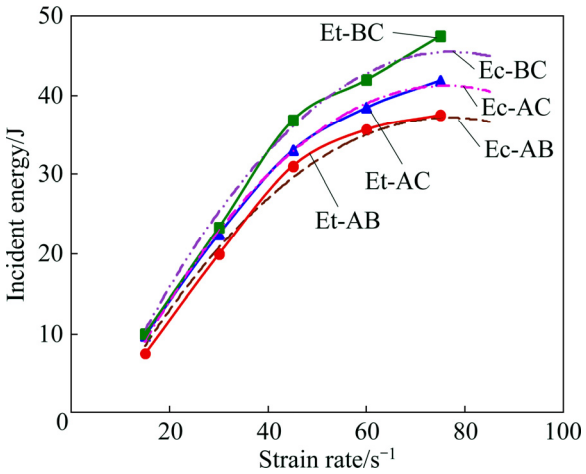

Fig. 11 Contrast curves of test results (Et) and calculation results (Ec) of incident energy

4 Conclusions

1) Dynamic compressive strength of LBS increases as the average cement content increases, and it shows evident strain rate effect. When strain rate is below the former intersected strain rate, dynamic compressive strength of LBS is smaller than that of corresponding single specimen with lower strength. When strain rate is over the latter intersected strain rate, dynamic compressive strength of LBS gets larger than that of corresponding single specimens with higher strength. The former and latter intersected strain rates of group AB, group AC and group BC of LBS are 48 s^{-1}/69 s^{-1}, 16 s^{-1}/79 s^{-1} and 45 s^{-1}/75 s^{-1}, respectively.

2) DSIF of LBS increases as strain rate increases. When strain rate ranges from 10 to 80 s^{-1}, DSIF of LBS ranges within 1.11−2.63.

3) Incident energy of LBS lies between that of the corresponding single backfill specimens while the energy dissipation rate of LBS is the largest compared with that of single backfill specimens. Under the same strain rate, incident energy of LBS decreases as the arithmetic average cement content increases.

4) Due to the layered structure of LBS, deformation degree of lower strength part is generally severer than that of strengthen part, and the results of numerical simulation give the same conclusion.

5) The average relative errors of results calculated by the revised failure criterion of LBS AB, AC and BC are 4.80%, 3.89% and 4.66%, respectively. The failure criterion based on incident energy is applicative to verdict the damage state of LBS.

References

[1] WANG Xin-min, ZHAO Bin, ZHANG Qin-li. Cemented backfill technology based on phosphorous gypsum [J]. Journal of Central South University, 2009, 16: 285−291.

[2] PENG Xin, LI Xi-bing, ZHANG Qin-li, WANG Xin-min. Quality evaluation of layer-like backfilling and flow pattern of backfill slurry in stope [J]. Journal of Central South University, 2007, 4: 580−583.

[3] DONG Yong-xiang, HUANG Chen-guang, DUAN Zhu-ping. Analysis on the influence of multi-layered media on stress wave propagation [J]. Chinese Journal of High Pressure Physics, 2005, 19(1): 59−65. (in Chinese)

[4] LIU Li, WANG Ze-yun, LIU Bao-xian. Study on damage constitutive relation of three-dimensional stratified composite rock [J]. Chinese Journal of Rock Mechanics and Engineering, 2002, 21(5): 621−625.

[5] DONG Kai-cheng. Research on the influence and control techniques of blasting seismic wave on backfill [D]. Changsha: Central South University, 2010. (in Chinese)

[6] DONG Wei, ZHOU Xiang-ming, WU Zhi-min. A fracture mechanics-based method for prediction of cracking of circular and

elliptical concrete rings under restrained shrinkage [J]. Engineering Fracture Mechanics, 2014, 131: 687−701.
[7] WANG Shi-ming. Experimental study on the mechanical properties and damage performance of early age concrete under dynamic loading [D]. Changsha: Central South University, 2014. (in Chinese)
[8] XIA Kai-wen, WEI Yao. Dynamic rock tests using split Hopkinson (Kolsky) bar system—A review [J]. Journal of Rock Mechanics and Geotechnical Engineering, 2015, 7(1): 27−59.
[9] ALBERTINI C, MONTAGNANI M. Testing techniques based on the split Hopkinson bar [M]. Ispra, Italy: EURATOM, 1974: 23−27.
[10] HONG Ling, LI Xi-bing, LIU Xi-ling, ZHOU Zi-long, YE Zhou-yuan, YIN Tu-bing. Stress uniformity process of specimens in SHPB test under different loading condition of rectangular and half-sine input waves [J]. Transactions of Nonferrous Metals Society of China, 2008, 18(2): 450−456.
[11] KUMAR A. The effect of stress rate and temperature on the strength of basalt and granite [J]. Geophysics, 1968, 33(10): 501−510.
[12] RINEHART J S. Dynamic fracture strengths of rocks [C]// Proceedings of 7th Symposium on Rock Mechanics. Canads: Mines Branch, 1965: 205−208.
[13] XIAO Shi-yun, ZHANG Jian. Compressive damage experiment of concrete at different strain rates [J]. China Civil Engineering Journal, 2010, 43(3): 40−45.
[14] BISCHOFF P, PERRY S. Impact behavior of plain concrete loaded in uniaxial compression [J]. Journal of Engineering Mechanics, 1995, 121(6): 685−693.
[15] OLSSON W A. The compressive strength of tuff as a function of strain rate from 10^{-6} to 10^{3}/sec [J]. International Journal of Rock mechanics and Mining Science & Geomechanics Abstract, 1991, 28(1): 115−118.
[16] BISCHOFF P. Compressive behaviour of concrete at high strain rates [J]. Materials and Structures, 1991, 24: 425−450.
[17] LIU Peng, GUAN Ping, WANG Huai-liang. Research progress of strain rate on dynamic strength properties of concrete [J]. Journal of Dalian University, 2009, 30(6): 79−84. (in Chinese)
[18] TEDESCO J W, ROSS C A. Strain-rate-dependent constitutive equations for concrete [J]. Journal of Pressure Vessel Technology, 1998, 120(4): 398−405.
[19] LI Xi-bing. Rock dynamics: fundamentals and applications [M]. Beijing, China: Science Press, 2014. (in Chinese)
[20] YIN Tu-bing, SHU Rong-hua, LI Xi-bing, WANG Pin, DONG Long-jun. Combined effects of temperature and axial pressure on dynamic mechanical properties of granite [J]. Transactions of Nonferrous Metals Society of China, 2016, 26: 2209−2219.
[21] YAN Pei-yu, QIN Xiao, YANG Wen-yan. Decomposition and delayed formation of ettringite in shrinkage-compensating massive concrete [J]. Journal of The Chinese Ceramic Society, 2000, 28(4): 319−325. (in Chinese)
[22] ONIFADE I, BIRGISSON B, BALIEU R. Energy-based damage and fracture framework for viscoelastic asphalt concrete [J]. Engineering Fracture Mechanics, 2015, 145: 67−85.
[23] OZBOLT J, BEDE N, SHARMA A, MAYER U. Dynamic fracture of concrete L-specimen: Experimental and numerical study [J]. Engineering Fracture Mechanics, 2015, 148: 27−41.
[24] LEI Ming, LIAO Hong-jian. Study on characters of stress wave propagation in functionally graded soil [J]. Chinese Journal of Rock Mechanics and Engineering, 2005, 24 (1): 4798−4804. (in Chinese)
[25] STEVERDING B, LEHNIGK S H. Response of cracks to impact [J]. Journal of Applied Physics, 1970, 41(5): 2096−2099.
[26] STEVERDING B, LEHNIGK S H. Collision of stress pulses with obstacles and dynamic of fracture [J]. Journal of Applied Physics, 1971, 42(8): 3231−3238.

中等应变率条件下分层充填体的动态力学特性及失稳特征

张云海，王新民，魏 冲，张钦礼

中南大学 资源与安全工程学院，长沙 410083

摘 要：为了得到应变率为 10~80 s^{-1} 的动载条件下分层充填体的动态力学特性及变形破坏规律，利用分离式 Hopkinson 杆系统对其进行冲击加载实验。实验结果表明，分层充填体的动态抗压强度及动态强度增长因子与应变率均存在正相关关系。分层充填体的动态抗压强度随着算术平均灰砂比的增加而增大，与静态抗压强度相比，分层充填体的动态峰值强度增加了 11%~163%。此外，分层充填体的能量吸收率随着水泥平均含量的升高而降低，且介于组成分层充填体的单体试块之间。分层充填体的形变表现出了不连续性，其强度较低的部分形变程度大于强度较高的部分。为了分析分层充填体试块的稳定性状态，利用基于 Stenerding−Lehnigk 准则推导出的改进方程来判断分层充填体的失稳条件，计算结果与 3 组试验结果的误差仅为 4.80%、3.89% 和 4.66%。

关键词：分层充填体试块；分离式霍普金森杆；动态力学特性；损伤特性；失稳判据

(Edited by Xiang-qun LI)